ChemComm

COMMUNICATION

View Article Online
View Journal | View Issue



Cite this: *Chem. Commun.*, 2024, **60**, 13690

Received 21st September 2024,
Accepted 28th October 2024

DOI: 10.1039/d4cc04902k

rsc.li/chemcomm



# Detecting single-point isomeric differences in polymer chains by MOF column chromatography†

Nobuhiko Hosono,*[a] Yu Kono,[a] Nagi Mizutani,‡[b] Daichi Koga[b] and Takashi Uemura*[a]

**Liquid chromatography with a metal–organic framework (MOF) as the stationary phase enables nanopore threading-based recognition of polymers and identification of single-point isomeric structural differences in the polymer main chain. The polymer adsorption affinity to the MOF and transient kinetics of polymer insertion into the nanopores play crucial roles in the recognition process.**

Advancements in polymer chemistry have led to increasingly complex polymer structures, heightening the need for precise separation techniques. Liquid chromatography (LC) remains the most widely used method for polymer separation and analysis.[1] However, distinguishing polymers with microstructural differences using traditional LC modes, such as the normal/reverse phase, interaction, and size-exclusion, is challenging. These modes typically recognise the physical properties of the entire molecule rather than directly accessing the chemical structure of the polymer chain. This limitation necessitates the development of new separation principles capable of targeting the local structures of polymer chains to detect the differences, mutations, and errors hidden within large macromolecular structures.

Metal–organic frameworks (MOFs) are porous crystalline compounds formed *via* the self-assembly of organic ligands and metal ions.[2,3] They are unique considering that various characteristics, such as the pore size, channel structure, and pore environment, can be tailored by adjusting the structure of the selected molecular components.[4,5] Owing to their highly flexible design, nearly $10^5$ MOFs have been synthesised,[6] with applications in a wide range of areas, including gas separation and storage,[7,8] heterogeneous catalysis,[9,10] and sensing.[11,12] These features have also been utilised in studies using MOFs as the stationary phase in LC, primarily to separate low molecular weight (MW) compounds such as hydrocarbons,[13–18] aromatics,[19–22] fullerenes,[23] and racemates.[24,25]

We recently demonstrated that MOF nanopores are promising for the polymer recognition of macromolecules.[26,27] We successfully separated polymers based on their adsorption to MOFs using a MOF-packed column; this method recognises even slight structural differences at the polymer termini[28] or in their topology[29] during the adsorption equilibrium of the polymer chain into the MOF nanopores,[30] resulting in varying retention times on the LC chromatograms (Fig. 1(a)). However, the capability of MOFs to detect extremely subtle structural mutations in the middle of a polymer chain remains unclear, which has been a long-standing challenge in polymer chemistry and analysis.

In this study, we demonstrated that an LC column filled with the MOF $[Zn_2(ndc)_2(ted)]_n$ (hereafter referred to as **1**;

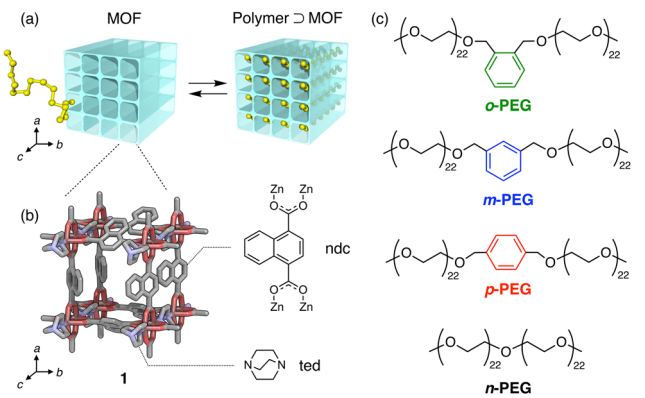


Fig. 1 (a) Schematic illustration of the nanopore threading-based polymer adsorption into a MOF. (b) Structure of MOF **1**, $[Zn_2(ndc)_2ted]_n$. The pseudo-1D channel open for polymer insertion directs to the *c*-axis of the MOF. (c) Chemical structures of the model PEGs possessing an *ortho*, *meta*, and *para*-substituted xylene moiety at the centre (***o*-PEG**, ***m*-PEG**, and ***p*-PEG**, respectively) and non-functionalized PEG (***n*-PEG**).

[a] *Department of Applied Chemistry, Graduate School of Engineering, The University of Tokyo, 7-3-1 Hongo, Bunkyo-ku, Tokyo 113-8656, Japan. E-mail: nhosono@g.ecc.u-tokyo.ac.jp, uemurat@g.ecc.u-tokyo.ac.jp*
[b] *Department of Advanced Materials Science, Graduate School of Frontier Sciences, The University of Tokyo, 5-1-5 Kashiwanoha, Kashiwa, Chiba 277-8561, Japan*

† Electronic supplementary information (ESI) available: Synthesis of compounds, powder X-ray diffractions, microscopy images, chromatograms, and adsorption kinetics data. See DOI: https://doi.org/10.1039/d4cc04902k

‡ Present address: AIST Chubu, National Institute of Advanced Industrial Science and Technology, 4-205, Sakurazaka, Moriyama-ku, Nagoya, Aichi 463-8560, Japan.

ndc = 1,4-naphthalenedicarboxylate, ted = triethylenediamine) (Fig. 1(b) and Fig. S1, S2, ESI†)[31] can identify a single-point phenyl mutation and its isomeric differences in the middle of a polyethylene glycol (PEG) chain (Fig. 1(c)). This was achieved by leveraging a nanopore threading-based adsorption process at the liquid/solid interface of the MOF stationary phase (Fig. 1(a)).

We prepared three PEGs (***o***-, ***m***-, and ***p*-PEG**) as model polymers with a single xylene moiety positioned at the exact centre of the chain (Fig. 1(c) and Fig. S3, Table S1, ESI†). These PEGs differ in the substitution position of the xylene moiety, which can be *ortho*, *meta*, or *para*-substituted. Notably, their total molecular weight ($M_n$ ~ 2000 g mol$^{-1}$) and chemical compositions were identical because they were derived from the same monofunctionalised PEG precursor ($M_n$ ~ 1000 g mol$^{-1}$) *via* coupling either *o*-, *m*-, or *p*-dibromoxylene (see ESI†). For comparison, we also prepared non-functionalised PEG (***n*-PEG**) with the same molecular weight using the same PEG precursor (Fig. 1(c)). These PEGs demonstrated negligible differences in the retention times when analysed using typical size-exclusion chromatography (SEC), indicating that they have identical hydrodynamic size owing to their structural similarity (Fig. S3, ESI†).

MOF **1** has pseudo-one-dimensional (1D) pores of diameter 0.57 nm (Fig. 1(b))[31] that can accommodate PEG chains, as reported in our previous study.[30,32] The adsorption of PEG chains into the narrow 1D pores occurs spontaneously, accompanied by a conformational change in the PEG to an elongated form, despite its radius of gyration ($R_g$) being approximately 1.5 nm (for PEG with a molecular weight of 2000 g mol$^{-1}$),[33] which exceeds the pore diameter of **1**. Under these conditions, we anticipated that the xylene unit would impede the insertion and diffusion of the entire PEG chain into the pores, owing to the narrow pore diameter, leading to separation. We prepared a **1**-packed column of dimensions 4 mm I.D. × 150 mm L using the same method as previously reported (see ESI†).[28,34] We used the column on an HPLC system to analyse the four PEGs with *N*,*N*-dimethylformamide (DMF) as the eluent at 80 °C with a flow rate of 1.0 mL min$^{-1}$. Notably, the PEGs eluted from the **1** column at different retention times in the following order: ***o*-PEG** ($t_c$ = 0.40 min) < ***m*-PEG** ($t_c$ = 2.02 min) < ***p*-PEG** ($t_c$ = 2.63 min) < ***n*-PEG** ($t_c$ = 2.87 min) ($t_c$: corrected retention time) (Fig. 2 and Table S2, ESI†), demonstrating that the detection of a single-point mutation in the PEG chain and discrimination of its substitution modes were achieved using the MOF column.

Among the tested PEGs, ***o*-PEG** exhibited a significantly lower affinity for the **1** column, with the fastest $t_c$ of 0.40 min. To further investigate the interaction of each PEG with the stationary phase, we conducted an additional analysis by varying the column temperatures from 60 °C to 80 °C (Fig. 2). At higher temperatures, the ***m***-, ***p***-, and ***n*-PEGs** demonstrated decreased retention times, which is consistent with previous findings indicating that PEG adsorption onto **1** is an exothermic process.[30,32] However, the retention time of ***o*-PEG** remained unchanged despite being at higher temperatures, suggesting that ***o*-PEG** cannot effectively interact with stationary phase **1**. This may be owing to the bulkier *ortho*-substituted xylene unit hindering the insertion of the PEG chain into the MOF nanopores.

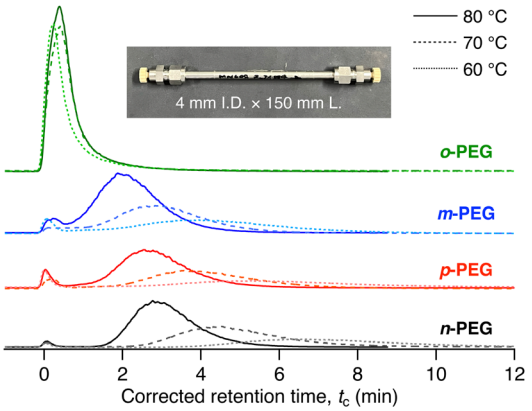


Fig. 2 HPLC chromatograms for ***o*-PEG** (green), ***m*-PEG** (blue), ***p*-PEG** (red), and ***n*-PEG** (black) on the **1**-packed column using DMF as the eluent at 80 °C (solid line), 70 °C (dashed line), and 60 °C (dotted line). The inset is a photograph of the **1**-packed column, demonstrating the dimensions. $t_c$ denotes the corrected retention time, $t_c = t_R - t_0$, where $t_R$ is the retention time and $t_0$ is the column hold-up time. For more detailed measurement conditions, see ESI.† A small front peak near $t_0$ is considered a breakthrough peak, which is occasionally observed in LC under certain conditions (see Fig. S4 in ESI†).[35,36]

Notably, the retention behaviour changed with the eluent flow rate. At a slower flow rate of 0.1 mL min$^{-1}$, ***o*-PEG** demonstrated a significant temperature dependence for its retention in the column (Fig. S4, ESI†). This observation indicates that the adsorption of ***o*-PEG** was not fully in equilibrium at higher flow rates. Thus, in addition to the thermodynamic factors, polymer insertion kinetics also play an important role in determining the retention behaviour and selectivity of polymers on the MOF column.

These findings led us to explore the relationship between the PEG retention and eluent flow rate. We calculated the retention factors, $k = (t_R - t_0)/t_0$, where $t_R$ is the retention time and $t_0$ is the hold-up time, for the four PEGs on the **1** column at six different flow rates (0.03, 0.1, 0.3, 0.5, 0.7, and 1.0 mL min$^{-1}$). All PEGs showed a decrease in $k$ as the flow rate increased. Notably, ***o*-PEG** displayed the strongest flow-rate dependence among the tested PEGs (Fig. 3(a)), with almost no retention at higher flow rates and a sharp increase in $k$ below 0.1 mL min$^{-1}$. In contrast, ***m***-, ***p***-, and ***n*-PEGs** showed modest, steady decreases in $k$ as the flow rate increased (Fig. 3(a)).

Theoretically, the retention factor ($k$) should remain constant regardless of the eluent flow rate. However, the observed $k$ values for the PEGs varied with flow rate (Fig. 3(a)). This variation could be attributed to the slow kinetics of polymer insertion into the MOF nanopores,[30] preventing the adsorption equilibrium from being fully established under the given flow and temperature conditions. To show the ability of the column to recognise microstructural differences, we calculated the $k$ ratios of the functionalised PEGs to the non-functionalised ***n*-PEG** ($A = k/k_{n\text{-PEG}}$) at different flow rates (Fig. 3(b)). The $A$ value remained constant across the tested flow rates for ***m*-PEG** and ***p*-PEG**; only ***o*-PEG** exhibited a pronounced flow-rate dependence. The $A$ value, which indicates the separation factor relative to ***n*-PEG**, demonstrated a significant increase in the

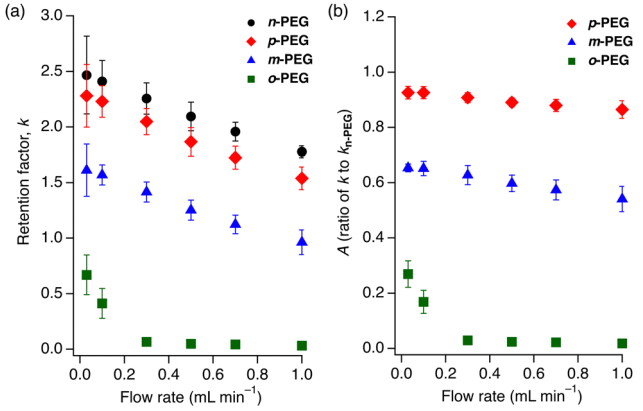


Fig. 3 Flow rate dependence of (a) $k$ for ***n*-PEG** (black circles), ***p*-PEG** (red diamonds), ***m*-PEG** (blue triangles) and ***o*-PEG** (green squares); and (b) $A$ ($k/k_{n\text{-PEG}}$) for ***p*-PEG** (red diamonds), ***m*-PEG** (blue triangles), and ***o*-PEG** (green squares). $A$ is a $k$ ratio of the functionalised PEG to ***n*-PEG**. Eluent: DMF at 80 °C. The measurement conditions are identical to those employed in Fig. 2.

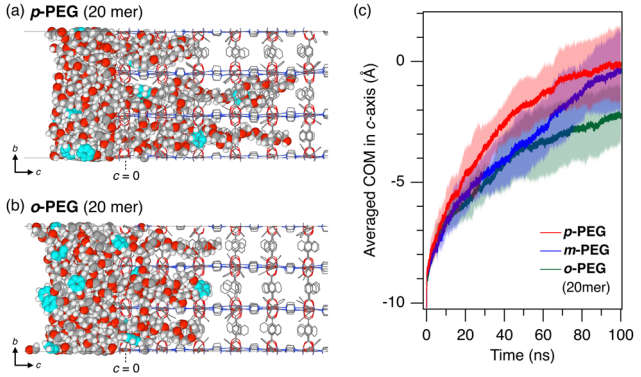


Fig. 4 Representative MD snapshots of (a) ***p*-PEG** and (b) ***o*-PEG** after 100-ns infiltration from the *ab* surface of **1** at 393 K; shortened versions of the PEGs were used (20 mer). For more detailed simulation conditions, see ESI.† The framework of **1** and PEGs are depicted using wireframes and space-filling models, respectively. Hydrogen atoms of the framework are omitted for clarity. Xylene unit in the PEG chain is coloured aqua blue. (c) Time evolution of the averaged COM of ***p*-PEG** (red), ***m*-PEG** (blue), and ***o*-PEG** (green) in the $c$-axis of **1**. The origin ($c$ = 0) is defined as the COM of Zn dimers of the paddle wheel cluster at the PEG/**1** interface. Averaged data from the five MD simulation runs are plotted as solid lines with shaded error bands of $\sigma$ ($N$ = 5).

selectivity at higher flow rates owing to the deviation of ***o*-PEG** from the thermodynamic retention trend. This indicates that a faster eluent flow facilitates the separation of ***o*-PEG** over the other PEG derivatives.

The flow-rate dependence of ***o*-PEG** suggests that the steric hindrance at the midpoint of ***o*-PEG** impedes its diffusion and insertion into the pores of **1**, resulting in a weaker overall interaction between the polymer and MOF. Namely, PEGs with bulkier substituents do not have sufficient time to fully access the MOF nanopores to maximise interactions under faster eluent flow conditions. This effect enabled the exceptional separation of what can be described as ''isomers'' of polymers. This discovery offers a groundbreaking perspective in polymer chemistry, as the concept of structural isomers has rarely been considered for polymeric compounds because such subtle differences in a large molecule cannot be identified and separated using existing methods.

A previous study reported a similar flow-rate dependence in a MOF column using UiO-66 as the stationary phase for separating low molecular weight compounds.[37] The UiO-66 column exhibited varying selectivities for alkylbenzenes and polycyclic aromatic hydrocarbons, depending on the eluent flow rate. Although the exact separation mechanism was not fully understood, the separation was attributed to molecular diffusion within the micropores of UiO-66 through its narrow windows. Molecules larger than these pores are excluded from entering the MOF, leading to weak retention on the column. This effect is similar to that in SEC, where smaller molecules can access a greater portion of the adsorbent pores, resulting in a stronger retention than bulkier molecules. We believe that this diffusional effect was significantly amplified in our polymer/MOF system, enabling the exceptional separation of polymers.

To confirm the differences in PEG diffusion during the adsorption process, we measured the adsorption kinetics of ***o*-**, ***m*-**, and ***p*-PEG** into **1** in the solution phase (Fig. S5, ESI†). We dispersed the particles of **1** in an ethanol solution of each PEG at 40 °C and monitored the PEG concentration in the supernatant using $^1$H NMR (see ESI†). The time evolution of PEG adsorption clearly depended on the substitution position of the central xylene unit, demonstrating the following trend: ***p*-PEG** > ***m*-PEG** > ***o*-PEG** (Fig. S5, ESI†). This suggests that straight chains are more likely to enter the pores, leading to more effective interactions with the MOF.

Furthermore, molecular dynamics (MD) simulations confirmed the observed trend in the diffusion kinetics of ***o*-**, ***m*-**, and ***p*-PEG** (Fig. 4). To highlight the diffusional differences and reduce the calculation cost, we considered the infiltration of molten PEG into **1** under neat conditions at 393 K in the MD simulation. We also shortened the length of the model PEGs to 20 mer ($HO(CH_2CH_2O)_{10}CH_2C_6H_4CH_2O(CH_2CH_2O)_{10}H$, see ESI†) to accelerate the simulations. The 100-ns initial infiltration from the surface of **1** was simulated for the respective PEG models. The centre of mass (COM) of each PEG molecule was calculated and the average COM on the $c$-axis of **1** was plotted as a function of the simulation time, as shown in Fig. 4(c) (Fig. S6, ESI†). The results showed that ***p*-PEG** diffused more quickly through the nanopores of **1**, whereas ***o*-PEG** diffused the slowest, likely owing to the higher energy barrier faced by the *ortho*-xylene centre when entering the 1D pore compared with the more linear-shaped xylene centres in other PEGs. These diffusional differences, as demonstrated by the experiments and simulations, provide a reasonable explanation for the kinetics-driven selectivity observed in the **1** column. In the MD simulations, ***m*-PEG** exhibited intermediate behaviour between ***o*-PEG** and ***p*-PEG**, with a slightly different diffusion pattern (Fig. 4(c)). It demonstrated a slow diffusion similar to that of ***o*-PEG** at the start of insertion but then nearly accelerated to that of ***p*-PEG** by the end of the 100-ns simulation. This suggests the presence of an energy barrier when entering the pores from the surface, followed by a pore diffusion comparable to that of ***p*-PEG**.[28]

On the **1** column, ***p*-PEG** and ***m*-PEG** showed the same slope of the flow-rate dependence (Fig. 3(a)), while showing a significant difference in their $k$ values. This suggests that kinetics-driven selectivity alone cannot fully explain the observed differences in the retention behaviour. Thus, their separation behaviour not only likely stems from the kinetic factors, but also from the thermodynamic factors of the PEG adsorption in **1**. This difference may be owing to the conformational change required for the adsorption of ***m*-PEG**, which has a kinked configuration at the central xylene unit, into the narrow 1D pores of **1**. This introduces a potential energy loss for the adsorption of ***m*-PEG**, leading to a weaker interaction with **1** than that of ***p*-PEG**. Further investigation is required to fully understand the nanopore-threading separation mechanism in MOF column chromatography, and comprehensive kinetic and thermodynamic analyses will be presented in future studies.

In conclusion, we revealed the unprecedented ability of a MOF-packed LC column to successfully separate PEGs based on the microstructural differences in their main chains. Our findings indicate that the separation mechanism is strongly influenced by kinetic factors, which leads to flow-rate-dependent selectivity, enhancing the separation performance of the MOF column and enabling it to detect single-point mutations and even more fine ''isomeric'' differences in polymer structures. This study highlighted the potential of MOF columns for recognising various microstructures in polymers. By incorporating the flow rate as a key parameter in the separation analysis with MOF columns, more diverse and advanced macromolecule separation techniques can be foreseen. Future developments in MOF-based nanopore-threading recognition will enable the separation of biomacromolecules, such as DNA and peptides, with minor structural differences.

This work was supported by JSPS KAKENHI Grant Numbers JP24K01535, JP24K21817, 22KJ0643, and JP21H04687. It was also supported by MEXT KAKENHI, grant Number JPMXP1122714694 (Data Creation and Utilization-Type Material Research and Development Project), and Japan Science and Technology Agency (JST) as part of Adopting Sustainable Partnerships for Innovative Research Ecosystem (ASPIRE), grant number JPMJAP2315. The authors thank Dr. Masayoshi Takayanagi (The Institute of Statistical Mathematics) for his guidance in constructing the force field dataset of **1** for the MD simulations, which were conducted using the facilities of the Supercomputer Center, the Institute for Solid State Physics, the University of Tokyo and the SuperComputer System, Institute for Chemical Research, Kyoto University.

## Data availability

The data supporting this article have been included as part of the ESI.†

## Conflicts of interest

There are no conflicts to declare.

## References

1 E. Uliyanchenko, S. van der Wal and P. J. Schoenmakers, *Polym. Chem.*, 2012, **3**, 2313–2335.
2 S. Kitagawa, R. Kitaura and S. Noro, *Angew. Chem., Int. Ed.*, 2004, **43**, 2334–2375.
3 M. J. Kalmutzki, N. Hanikel and O. M. Yaghi, *Sci. Adv.*, 2018, **4**, eaat9180.
4 O. Yaghi, M. O'keeffe, N. Ockwig, H. Chae, M. Eddaoudi and J. Kim, *Nature*, 2003, **423**, 705–714.
5 H. Jiang, D. Alezi and M. Eddaoudi, *Nat. Rev. Mater.*, 2021, **6**, 466–487.
6 P. Z. Moghadam, A. Li, S. B. Wiggin, A. Tao, A. G. P. Maloney, P. A. Wood, S. C. Ward and D. Fairen-Jimenez, *Chem. Mater.*, 2017, **29**, 2618–2625.
7 H. Wang, Q.-L. Zhu, R. Zou and Q. Xu, *Chem*, 2017, **2**, 52–80.
8 B. Li, H.-M. Wen, W. Zhou, J. Q. Xu and B. Chen, *Chem*, 2016, **1**, 557–580.
9 H. G. T. Ly, G. Fu, A. Kondinski, B. Bueken, D. D. Vos and T. N. Parac-Vogt, *J. Am. Chem. Soc.*, 2018, **140**, 6325–6335.
10 L. Zhang, X. Shi, Z. Zhang, R. P. Kuchel, R. Namivandi-Zangeneh, N. Corrigan, K. Jung, K. Liang and C. Boyer, *Angew. Chem., Int. Ed.*, 2021, **60**, 5489–5496.
11 Z. Meng, R. M. Stolz, L. S. D. Moraes, C. G. Jones, A. M. Eagleton, H. M. Nelson and K. A. Mirica, *Angew. Chem., Int. Ed.*, 2024, **63**, e202404290.
12 L. E. Kreno, K. Leong, O. K. Farha, M. Allendorf, R. P. V. Duyne and J. T. Hupp, *Chem. Rev.*, 2012, **112**, 1105–1125.
13 Z.-Y. Gu, C.-X. Yang, N. Chang and X.-P. Yan, *Acc. Chem. Res.*, 2012, **45**, 734–745.
14 S.-S. Liu, C.-X. Yang, S.-W. Wang and X.-P. Yan, *Analyst*, 2012, **137**, 816–818.
15 J. Zhang, J. Chen, S. Peng, S. Peng, Z. Zhang, Y. Tong, P. W. Miller and X.-P. Yan, *Chem. Soc. Rev.*, 2019, **48**, 2566–2595.
16 A. A. Kotova, D. Thiebaut, J. Vial, A. Tissot and C. Serre, *Coord. Chem. Rev.*, 2022, **455**, 214364.
17 K. Yusuf, A. Aqel and Z. ALOthman, *J. Chromatogr. A*, 2014, **1348**, 1–16.
18 S. V. der Perre, A. Liekens, B. Bueken, D. E. D. Vos, G. V. Baron and J. F. M. Denayer, *J. Chromatogr. A*, 2016, **1469**, 68–76.
19 M. Maes, F. Vermoortele, L. Alaerts, S. Couck, C. E. A. Kirschhock, J. F. M. Denayer and D. E. D. Vos, *J. Am. Chem. Soc.*, 2010, **132**, 15277–15285.
20 L. Alaerts, M. Maes, L. Giebeler, P. A. Jacobs, J. A. Martens, J. F. M. Denayer, C. E. A. Kirschhock and D. E. D. Vos, *J. Am. Chem. Soc.*, 2008, **130**, 14170–14178.
21 L. Alaerts, M. Maes, M. A. van der Veen, P. A. Jacobs and D. E. D. Vos, *Phys. Chem. Chem. Phys.*, 2009, **11**, 2903–2911.
22 C.-X. Yang and X.-P. Yan, *Anal. Chem.*, 2011, **83**, 7144–7150.
23 C.-X. Yang, Y.-J. Chen, H.-F. Wang and X.-P. Yan, *Chem. – Eur. J.*, 2011, **17**, 11734–11737.
24 M. Zhang, X.-D. Xue, J.-H. Zhang, S.-M. Xie, Y. Zhang and L.-M. Yuan, *Anal. Methods*, 2013, **6**, 341–346.
25 H. Jiang, K. Yang, X. Zhao, W. Zhang, Y. Liu, J. Jiang and Y. Cui, *J. Am. Chem. Soc.*, 2021, **143**, 390–398.
26 N. Hosono and T. Uemura, *Matter*, 2020, **3**, 652–663.
27 N. Hosono and T. Uemura, *Acc. Chem. Res.*, 2021, **54**, 3593–3603.
28 N. Mizutani, N. Hosono, B. Le Ouay, T. Kitao, R. Matsuura, T. Kubo and T. Uemura, *J. Am. Chem. Soc.*, 2020, **142**, 3701–3705.
29 T. Sawayama, Y. Wang, T. Watanabe, M. Takayanagi, T. Yamamoto, N. Hosono and T. Uemura, *Angew. Chem., Int. Ed.*, 2021, **60**, 11830–11834.
30 N. Oe, N. Hosono and T. Uemura, *Chem. Sci.*, 2021, **12**, 12576–12586.
31 H. Chun, D. N. Dybtsev, H. Kim and K. Kim, *Chem. – Eur. J.*, 2005, **11**, 3521–3529.
32 B. Le Ouay, C. Watanabe, S. Mochizuki, M. Takayanagi, M. Nagaoka, T. Kitao and T. Uemura, *Nat. Commun.*, 2018, **9**, 3635.
33 K. A. Rubinson and S. Krueger, *Polymer*, 2009, **50**, 4852–4858.
34 K. Kioka, N. Mizutani, N. Hosono and T. Uemura, *ACS Nano*, 2022, **16**, 6771–6780.
35 S. Chapel, F. Rouvière, V. Peppermans, G. Desmet and S. Heinisch, *J. Chromatogr. A*, 2021, **1653**, 462399.
36 X. Jiang, A. van der Horst and P. J. Schoenmakers, *J. Chromatogr. A*, 2002, **982**, 55–68.
37 A. Peristyy, P. N. Nesterenko, A. Das, D. M. D'Alessandro, E. F. Hilder and R. D. Arrua, *Chem. Commun.*, 2016, **52**, 5301–5304.